ELSEVIER

Earth and Planetary Science Letters 184 (2001) 703–718

EPSL

www.elsevier.com/locate/epsl

Crystal and magma residence at Kilauea Volcano, Hawaii: ^{230}Th–^{226}Ra dating of the 1955 east rift eruption

Kari M. Cooper [a,b,*], Mary R. Reid [a], Michael T. Murrell [b], David A. Clague [c]

[a] *Department of Earth and Space Sciences, UCLA, 595 Charles Young Drive East, Los Angeles, CA 90095-1567, USA*
[b] *Los Alamos National Laboratory, P.O. Box 1663, MS J514, Los Alamos, NM 87545, USA*
[c] *Monterey Bay Aquarium Research Institute, P.O. Box 628, 7700 Sandholdt Road, Moss Landing, CA 95039, USA*

Received 29 March 2000; received in revised form 26 October 2000; accepted 2 November 2000

Abstract

Previous estimates of crustal storage time of magmas at Kilauea Volcano, Hawaii, range from a few years to a few thousand years, leading to considerable uncertainty in the time scales of processes of magmatic storage and differentiation. We present a new approach for determining minimum magma residence times which involves dating phenocrysts in a magma using ^{226}Ra–^{230}Th disequilibria, and apply this approach to the early phase of the 1955 east rift eruption at Kilauea. When fractionation of Ra from Ba (a proxy for initial Ra in the crystals) during crystal growth is considered along with the effects of inclusions in the minerals, the data are consistent with co-precipitation of plagioclase and clinopyroxene from a melt represented by the groundmass at a mean age of 1000^{+300}_{-400} a. Unless a significant fraction ($>30\%$) of the crystals are remnants from an earlier batch of evolved magma in the system, these data constrain the minimum magmatic residence time to be $\sim$550 yr, considerably longer than most previous estimates of storage time at Kilauea as well as those for some other basaltic systems. For the temperature interval of augite+plagioclase growth in the early 1955 magma, a maximum constant cooling rate of 0.1°C/yr (1×10^{-5}°C/h) is derived from the minimum magmatic residence time of 550 yr. The total magma storage time would be >2500 yr if this cooling rate applied to the entire thermal history of the magma, although a more complex cooling history where cooling rates were more rapid early in the storage history is permissive of a total residence time which is not much longer than 550 yr. The disparate estimates of magma residence at Kilauea may reflect the uncertainties in the methods of estimation in addition to true variations in storage time for different batches of magma. More work is necessary in order to determine whether a long residence time is characteristic of rift zone lavas and/or of Kilauean lavas in general.

Keywords: Kilauea; Th-230/Ra-226; residence time

1. Introduction

The residence time of magma in crustal reservoirs has implications for our understanding of rates of crystal growth and magmatic differentiation, and for the thermal regime of magma reser-

* Corresponding author. Tel.: +1-310-206-1938; Fax: +1-310-825-2779; E-mail: kcooper@ess.ucla.edu

0012-821X/01/$ – see front matter
PII: S0012-821X(00)00341-1

voir systems. The time scales of such processes are difficult to quantify and, for Hawaiian volcanoes in particular, estimates are quite disparate. Some of the range in ages may reflect the fact that the different methods average residence times over different time and length scales, such that estimates range from ~10 yr for the last part of the storage history of a single batch of magma [1] based on crystal size distributions, to an average residence time of 90–180 and 30–40 yr based on geochemical variations in magmas erupted at the summit during the early and late 20th century, respectively [2], to an average residence time of 100–3000 yr [3,4] for the entire interconnected volume of the magma reservoir system beneath Kilauea based on geophysical estimates of reservoir size and magma supply rate. Furthermore, few estimates of residence time for magmas erupted from Kilauea's rift zones exist, although an estimate of 7–14 yr [5] is an average for Puu Oo lavas based on temporal changes in geochemistry.

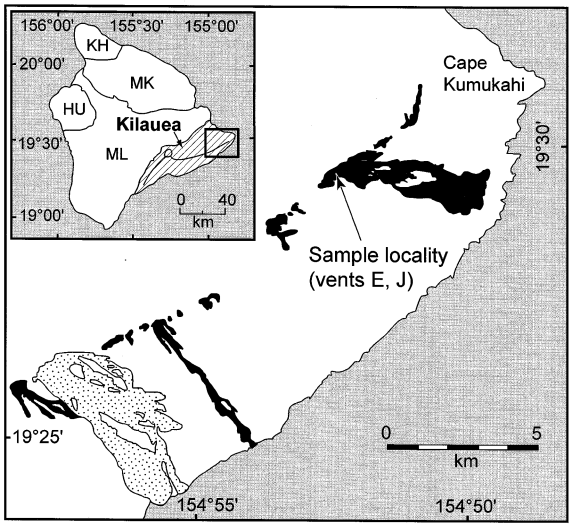

Fig. 1. Map showing extent of the flows of the 1955 east rift eruption and sample locality (after [11]). Early flows shown in black, late flows in stippled pattern. Inset shows index map of the island of Hawaii, showing the boundaries between volcanoes, abbreviated as follows: KH, Kohala; MK, Mauna Kea; HU, Hualalai; and ML, Mauna Loa. Kilauea is shown in the ruled pattern, along with its summit (small circle) and rift zones (curved lines radiating from summit region), after [33]. Box indicates area shown in main figure.

Our approach to constraining residence times of Hawaiian magmas is the first direct measurement of magma residence in Kilauea's east rift reservoir and is based on ^{230}Th–^{226}Ra dating of mineral and groundmass separates from lavas. The magnitude of disequilibrium between ^{230}Th and its immediate daughter ^{226}Ra ($t_{1/2}$ = 1600 yr) is a function of the initial fractionation of Ra from Th and of the time elapsed since crystal growth. One underlying uncertainty in this approach results from the fact that no longer-lived isotope of Ra exists. In this study, we evaluate potential complications involved in the standard assumption that the magnitude of crystal–liquid fractionation of Ba can be used to delimit the amount of ^{226}Ra incorporated initially by the crystal. By accounting for these uncertainties, we obtain a minimum age of crystallization. From this, we determine a minimum magmatic residence time for the early stage of the 1955 east rift eruption of Kilauea, which will apply unless the magma contains a large (>30%) proportion of old xenocrysts.

2. Geological background

The location, size and shape of Kilauea's reservoir system is inferred from the locus of eruptions, the distribution of aseismic zones within the volcanic edifice [6], geodesy (e.g., [4]), and chemical variations in erupted lavas [2,7,8]. Shallow storage of magma at Kilauea takes place in a relatively equant summit reservoir, the top of which is 2–4 km below the surface, and also in dike-like bodies beneath the rift zones which extend radially from the summit reservoir, and from near-surface to ~9 km depth (e.g., [6,9]). In detail, the size, shape, and degree of interconnectivity of the summit and rift reservoirs are poorly constrained (e.g., [2–4,10]), resulting in uncertainty about the extent to which the magma reservoirs can be considered physically and chemically well-mixed.

The data presented in this study are for a sample of the early phase of Kilauea's 1955 east rift eruption collected near vents E and J (Fig. 1; vent nomenclature of [11]). This phase of the eruption

produced some of the most evolved lavas erupted at Kilauea, with compositions ranging from 5.0 to 5.7 wt% MgO [7,11]. After approximately half of the $\sim$0.1 km^3 total volume of the 1955 lava had erupted, the composition changed abruptly to the more magnesian (6.2–6.8% MgO) lavas characteristic of the late 1955 eruption [11,12], and eruptive activity localized at a restricted number of up-rift vents (Fig. 1). The early and late 1955 lavas have been interpreted to be related by crystal fractionation on the basis of modeling of major and trace element characteristics of erupted lavas [13]. However, more recent work [14] re-evaluated this conclusion based on extensive petrographic work combined with additional major and trace element analyses, and concluded that the late 1955 lavas were best modeled as a mixture of early 1955 compositions with a more primitive component similar to the 1952 summit lava. The early 1955 magma appears unaffected by mixing with this primitive magma. However, reverse zoning and rounding of oxide phenocrysts suggest that the early 1955 magma could have formed by mixing of two highly differentiated magmas [15]. If magma mixing occurred, the two components were probably thermally and chemically similar because compositions and textural relations of the majority of silicate phenocrysts are consistent with equilibrium between crystals and melt.

We chose the early 1955 lava for analysis because its differentiated nature is well-documented and makes it a good candidate for having experienced a measurable (longer than a few tens of years) residence time. The 1955 eruption was the first eruption on the lower east rift zone of Kilauea in over 100 years, and followed by 31 years the last intrusion recorded in the rift zone (in 1924 [7]). Thus, if the early 1955 lava was stored in the rift zone prior to eruption, its storage time was at least 31 years.

3. Results

3.1. U-series analyses of mineral separates

We measured Th and U isotopic compositions and abundances of Ra, Th, Ba, and U in mineral separates, groundmass, and whole rock samples of the early 1955 lava by TIMS; results are presented in Table 1, and analytical methods are described in Appendix A. $^{234}U/^{238}U$ activity ratios of all phases are within error of unity (2σ errors generally $\leq 0.5\%$), as expected for unaltered volcanic rocks. The abundances of Ra, Th, U, and Ba in the plagioclase and pyroxene separates are lower (by factors of 3–50) than those measured in the same phases from olivine basalt and andesite from Mount St. Helens [16] and the Ra abundance in the pyroxene separate represents the lowest reported to date for volcanic separates. This likely reflects the lower abundances of incompat-

Table 1
Ba, Ra, Th, U concentrations measured by TIMS and calculated Th, U, and Ra activities

Sample	Th	U	Ba	Ra	$\frac{(^{230}Th)}{(^{232}Th)}$	$\frac{(^{230}Th)}{(^{238}U)}$	$\frac{(^{226}Ra)}{(^{230}Th)}$	$\frac{(^{230}Th)}{Ba}$	$\frac{(^{226}Ra)}{Ba}$
	(μg/g)	(μg/g)	(μg/g)	(fg/g $\pm 2\sigma$)				(dpy/μg)	(dpy/μg)
97KC05 GM	1.780	0.606	196.3	233.6 ± 2.9	1.052	1.016	1.125	1221	1373
97KC05 WR	1.664	0.570	184.1	219.2 ± 1.6	1.040	0.997	1.142	1203	1375
97KC05 PL	0.01447	0.00372	45.8	9.12 ± 0.08	–	1.345	5.40	42.6	230
97KC05 PX	0.01453	0.00451	1.15	1.371 ± 0.018	1.045	1.105	0.814	1690	1376

U, Th, Ba, and Ra concentrations measured by isotope dilution thermal ionization mass spectrometry at LANL (see Appendix A for details). GM = groundmass, WR = whole rock, PL = plagioclase separate, PX = pyroxene separate. Measurement errors are $< 0.6\%$ for Th and U concentrations and $< 0.2\%$ for Ba concentrations (2σ). Parentheses denote activities, calculated using the following decay constants (all yr^{-1}): λ_{238} = 1.551E-10, λ_{230} = 9.158E-6, λ_{232} = 4.933E-11, λ_{226} = 4.332E-4. Th isotopic compositions measured by TIMS at LANL; errors (2σ) are $< 0.4\%$ in whole rock and groundmass measurements and 1.7% in pyroxene measurement. Th isotopic composition for plagioclase not determined; (^{230}Th) in plagioclase was calculated assuming that Th isotopic composition is equal to that measured in the groundmass; allowing (^{230}Th)/(^{232}Th) to vary between 1.035 and 1.09 (the range measured in historical Kilauea lavas by [17]) changes the (^{230}Th)/Ba value by $< 5\%$ and will have virtually no effect on calculated ages.

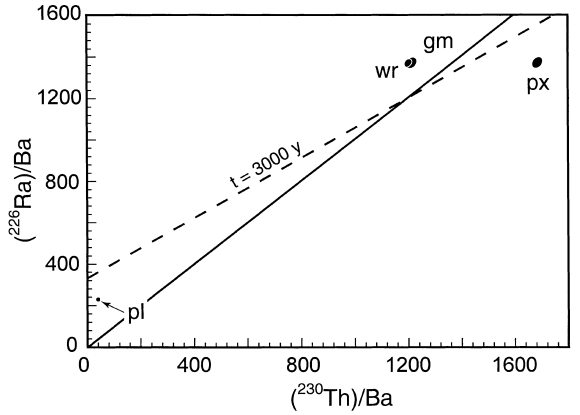

Fig. 2. Ba-normalized ^{226}Ra–^{230}Th isochron diagram showing groundmass (gm), pyroxene (px), plagioclase (pl), and whole rock (wr) data for the early 1955 eruption. The solid line represents ^{226}Ra–^{230}Th radioactive equilibrium (equiline); the dashed line is a 3 ka reference isochron for phases having the same initial (^{226}Ra)/Ba ratio. Sizes of symbols correspond to measurement uncertainty (2σ). Parentheses denote activities of ^{226}Ra and ^{230}Th (in disintegrations per year); denominator on both axes is concentration of Ba (μg/g).

ible elements in Hawaiian tholeiites compared to arc basalts. With respect to ^{230}Th, plagioclase is ^{226}Ra-enriched whereas pyroxene is ^{226}Ra-depleted, as expected from relative compatibility of Ba (and by extension Ra) and Th in these minerals (cf. [16]). The groundmass separate has (^{226}Ra)/(^{230}Th) = 1.13, similar to recent high-precision measurements of ^{226}Ra–^{230}Th disequilibria in Kilauea lavas (cf. [17,18]).

Data for the separates from the 1955 eruption are plotted on a ^{226}Ra–^{230}Th activity diagram in Fig. 2; activities of ^{226}Ra and ^{230}Th are normalized to Ba as a proxy for initial ^{226}Ra. The three separates show an overall correlation between (^{226}Ra)/Ba and (^{230}Th)/Ba, which would generally be interpreted as reflecting relative changes in (^{226}Ra)/Ba due to radioactive decay since crystallization. The slope of the best-fit line through these data corresponds to an age of 3.4 ka. The scatter in the data around a single isochron is greater than expected from the analytical uncertainties and could reflect differences in age between pyroxene, plagioclase and/or groundmass, and/or differences in the initial (^{226}Ra)/Ba of the three separates. For the first case to apply, the mean age of the pyroxene–groundmass pair (within error of eruption) would be considerably younger than that of the plagioclase–groundmass pair (8.1 ka).

3.2. In situ trace element analyses of pyroxene

We measured Th and Ba concentrations by ion microprobe in pyroxene grains from a split of the pyroxene separate analyzed by TIMS; in order to better interpret the data, major element compositions of the same grains were obtained by electron microprobe. Analytical details are presented in

Table 2
Ion microprobe analyses of Ba and Th in pyroxene

Sample	Ba		Th		Th/Ba
	(μg/g)	(±)	(μg/g)	(±)	
Augite:					
r1g2a	0.023	0.002	0.008	0.0008	0.34
r1g3a	0.020	0.002	0.004	0.0007	0.21
r1g4a	0.028	0.003	0.006	0.0009	0.22
r2g1a	0.020	0.002	0.008	0.002	0.38
r2g5a	0.035	0.004	0.006	0.001	0.18
Weighted mean	*0.023*	*0.001*	*0.006*	*0.0004*	*0.26*
MSWD	*4.9*		*3.7*		
Orthopyroxene:					
r3g3a_sp1	0.0009	0.0003	0.0024	0.0007	2.6
r3g3a_sp2	0.006	0.003	0.003	0.001	0.47

Concentrations of Ba and Th in pyroxene analyses were calculated with reference to WU-A standard; see Appendix A for instrumental conditions and details of calibration. Uncertainties are reported as one standard error.

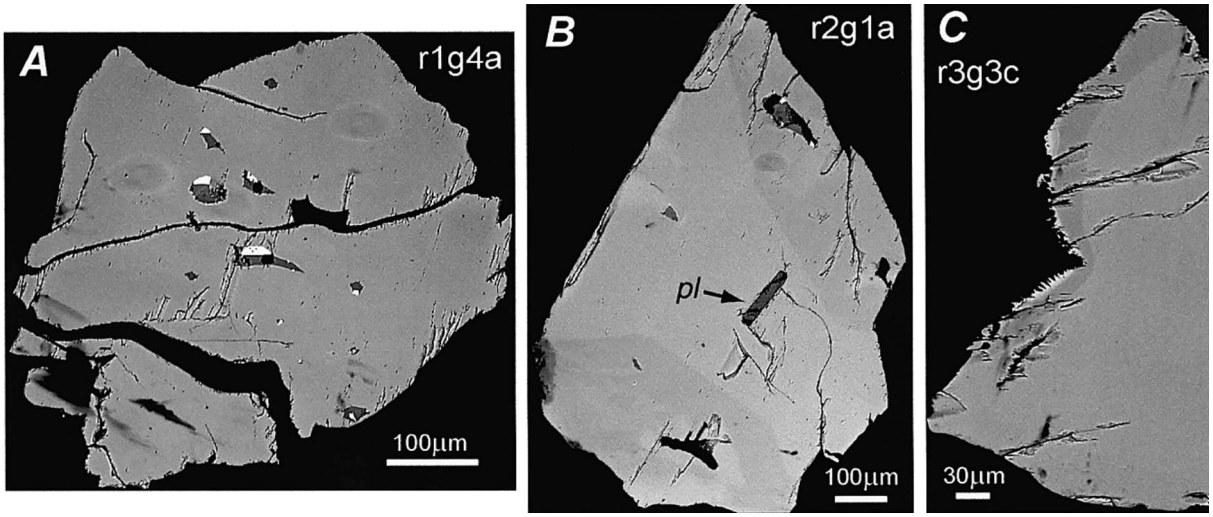

Fig. 3. BSE images of augite grains from the early 1955 east rift lava analyzed in this study. Faint dark ovals with lighter rims are ion microprobe analysis pits. A: Typical augite grain from the early 1955 lava with melt inclusions, now present as glass (dark gray) with some post-entrapment crystallization of Fe–Ti oxides (bright phase) and bubbles (black circles); lack of compositional zoning is characteristic of the majority of grains imaged. B: Plagioclase (pl) and melt inclusions in a sector-zoned augite grain. C: Sole example, of 25 grains studied, of a reversely zoned crystal with darker, more-magnesian rim (~30 μm thick on upper left grain margin; cf. Fig. 4). 'Fringe' at very edge of grain likely represents post-eruptive crystallization of augite intergrown with glass.

Appendix A. Weighted means of Th and Ba concentrations measured in five augite grains (Table 2) are 6.0 ± 0.4 ppb and 23 ± 1.0 ppb, respectively (1σ errors), substantially lower than the concentrations of 15 ppb Th and 1150 ppb Ba measured in the bulk separate by TIMS (cf. Table 1). The mean of two analyses of orthopyroxene is 2.6 ppb Th and 3.5 ppb Ba. The mean square of the weighted deviates (MSWD) for the augite analyses is greater than that expected for a single population (see Table 2), which may indicate that the true analytical precision is of the order of 25–30%, or that there is a ~15% variation in the Th and Ba concentrations of the augite grains. The corresponding compositional range of augite is $En_{50.3–42.7}Fs_{11.1–22.3}Wo_{34.0–41.7}$, and 100Mg/(Mg+$Fe^{2+}$) 66.6–81.5 (Fig. 4), which overlaps with and extends the range of compositions reported previously for the early 1955 lavas (cf. [13,15]).

Backscattered electron (BSE) imaging (Fig. 3) showed that inclusions of glass (partially crystallized in some cases to opaque minerals and/or pyroxene) were present in the plane of the section in approximately half of the crystals and one crystal also had a plagioclase inclusion (Fig. 3B). Thin films of microcrystalline groundmass were attached to the rims of a few of the crystals. The majority of the pyroxene grains imaged appeared unzoned, although a few grains did have a distinct, lighter-colored rim (e.g., Fig. 3C), likely representing post-eruptive crystallization.

4. Discussion

4.1. Differential partitioning of Ra and Ba

Previous studies using ^{226}Ra–^{230}Th mineral isochrons to constrain residence times (e.g., [16,19,20]) have assumed negligible fractionation of Ra from Ba during crystallization. If this model applied to the case of the 1955 lava, it would imply that the plagioclase was ~8 ka older than the augite. Large differences in the average age of augite and plagioclase are not expected, given the experimental observation that augite in Kilauean magmas should begin to crystallize at only slightly

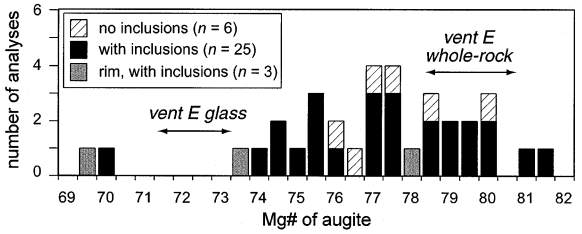

Fig. 4. Histogram of Mg# of augite grains analyzed by electron microprobe. Analyses labeled as rims include only those which are identified unequivocally as rims either by adhering groundmass or by zoning following the grain outlines (see Fig. 3); a few additional analyses from the edges of broken crystals, could potentially represent rims. Rim analysis with Mg# = 78.3 is from the dark rim of the reversely zoned grain shown in Fig. 3C. One analysis of the outermost rim of a pyroxene grain (Mg# = 66.6) likely represents post-eruptive crystallization and was omitted from this diagram. Range of augite Mg# that would be in equilibrium with vent E whole rock [13] and glass [15] compositions assume an Fe–Mg distribution coefficient of 0.25 for augite [34]. Full data are available from the first author upon request.

higher temperatures than plagioclase [21]. Differential removal or gain of plagioclase and augite from the system, to the extent that it would lead to different mean ages for the two phases, is inconsistent with the fact that the range in compositions in early 1955 lavas follows the Kilauean liquid line of descent [14].

Recent work modeling trace element partitioning [22–24] predicts that the ~5% difference in ionic radius between Ra and Ba will result in significantly different partition coefficients for the two elements in silicate minerals. Preferential exclusion of Ra relative to Ba from the crystals can qualitatively explain why our groundmass separate lies above the isochron defined by pyroxene and plagioclase separates in Fig. 2. Our results appear therefore to delimit the magnitude of this initial fractionation; however, to be meaningful, the effects of potential contaminants in the mineral separates must be considered. For the plagioclase separate, glass is the only potential contaminant that could significantly affect the Ba and Th concentrations measured by TIMS, and it can account for no more than 0.8% of the separate by mass balance calculations. The pyroxene separate contains documented impurities in the form of glass and plagioclase inclusions and adhering groundmass (e.g., Fig. 3), and could potentially include some olivine and oxides. When the concentrations of trace elements in those impurities are considered, only glass and plagioclase would be expected to contribute non-negligible quantities of Th and Ba (and, by extension, Ra) to the measured values. The pyroxene separate consists largely of augite but contains ~10–15% orthopyroxene, which, because concentrations of Th and Ba in orthopyroxene are so low, would have the effect of decreasing the measured concentrations relative to pure augite without greatly affecting measured interelement ratios. The total mass of Ba in the pyroxene separate can be accounted for by either 0.6% glass or 2.6% plagioclase. The best-fit percentages of 0.3% plagioclase and 0.5% glass, obtained by assuming 10–15% orthopyroxene and using the concentrations of Th and Ba measured in augite and orthopyroxene by ion microprobe and measured in the groundmass and plagioclase separates by TIMS, are qualitatively consistent with the abundance of glass inclusions observed in SEM images. An estimated concentration of 0.21 fg/g Ra in augite is given by accounting for the contribution of other phases to Ra in the pyroxene separate; this estimate assumes that the concentration of Ra in orthopyroxene is negligible and allows for the potential contribution of glass to the Ra content of the plagioclase separate. A minimum concentration of 0.03 fg/g Ra in augite is obtained by recognizing that because glass and plagioclase have (^{226}Ra)/Ba lower than that measured in the pyroxene separate, the augite must have (^{226}Ra)/Ba at least as high as that of the separate. A maximum concentration of 0.5 fg/g Ra in augite is obtained by assuming that plagioclase is the only contaminant.

Apparent partition coefficients derived from the foregoing considerations are given in Table 3. The effect of decay or ingrowth before eruption will be to decrease (plagioclase) or increase (pyroxene) Ra concentrations, so that the apparent D_{Ra} values calculated from our plagioclase–groundmass and augite–groundmass pairs represent minimum and maximum values, respectively. Ba and Th concentrations will be constant or effectively constant over the time scales of magma storage, but

because non-equilibrium effects and impurities in the separates would both tend to result in partition coefficients closer to one than in the pure phases at equilibrium, the apparent D_{Th} and D_{Ba} values calculated from our data likely represent maximum values for equilibrium partitioning.

4.2. Estimated crystallization ages

As we will show, the apparent magnitude of crystal–liquid fractionation of Ba and Ra is qualitatively reasonable, but when modeled quantitatively, cannot alone account for the pattern of data shown in Fig. 2. As reasoned above, the augite in the pyroxene separate must have a (^{226}Ra)/Ba higher than that measured in the separate as a whole and thus higher than the groundmass. If this relationship were solely the product of differential partitioning it would contradict most models of the relative crystal–liquid partitioning behavior of these two elements, given the greater ionic radius of Ra compared to Ba. We therefore consider it likely that (^{226}Ra)/Ba measured in our separates reflects not only initial Ra–Ba fractionation but also the effects of crystal aging prior to eruption.

To assess the possible duration of in situ ^{230}Th–^{226}Ra decay and the general validity of the apparent partition coefficients extrapolated from our measurements, we used the model developed in [22,24] to calculate partition coefficients for Ra and Ba in plagioclase and augite under conditions relevant to crystallization in the 1955 magma (Table 3); details of the parameters used in our calculations and a discussion of error estimation are given in Appendix B. Experimentally determined partition coefficients for Ba and Th are also given in Table 3 and these compare favorably to the apparent partition coefficients obtained in this study. As expected, the model results predict that Ra will be more incompatible than Ba (i.e., $D_{Ra}/D_{Ba} < 1$), and the magnitude of this fractionation will increase with decreasing temperature and increasing Ca content in both phases. Given these partition coefficients, rather than being similar to that of the melt from which they crystallize, initial (^{226}Ra)/Ba values in the crystals are expected to be significantly lower than the melt. Consequently, if the effect of differential partitioning were neglected, the plagioclase–groundmass apparent age would overestimate the age of crystallization, while the augite–groundmass apparent age would underestimate it. (^{226}Ra)/Ba is predicted to be approximately an order of magnitude

Table 3
Calculated, experimentally determined, and apparent partition coefficients

Phase/method	T (°C)	D^{a}_{Ra}	D_{Ba}	D_{Ra}/D_{Ba}	D_{Th}
Augite:					
Calculated	1100	1.19E-7	1.00E-5	0.012	–
Calculated	1160	2.67E-7	1.78E-5	0.015	–
Experimental	1190–1291	–	1.1E-4 to 4.7E-4	–	4.3E-3 to 4.1E-4
Apparent (*ion microprobe*)	1100–1160	*9.2E-4*	1.2E-4	*7.9*	3.4E-3
Plagioclase:					
Calculated (An_{70})	1100	4.54E-2	2.13E-1	0.21	–
Calculated (An_{70})	1160	5.17E-2	2.27E-1	0.23	–
Calculated (An_{60})	1100	6.73E-2	2.88E-1	0.23	–
Calculated (An_{60})	1160	7.53E-2	3.04E-1	0.25	–
Experimental	1100–1200	–	3.8E-1 to 1.5E0		1.3E-1 to 1.9E-1
Apparent (*TIMS data*)	1100–1160	*4.0E-2*	2.3E-1	*0.17*	8.1E-3

Calculated partition coefficients were modeled using the method of [22,24]; details of calculations reported in Appendix B. Experimentally determined partition coefficients shown for augite represent the range in D_{Th}/D_{Ba} for individual experiments of [36]; partition coefficients for diopside determined by [35] fall within this range, and partition coefficients for augite determined by [37] were not used because their D_{Th} was greater than apparent D_{Th} in our samples. Experimental partition coefficients for plagioclase from [38]. Apparent partition coefficients calculated from measured mineral and groundmass concentrations (this study).

[a]Note that apparent partition coefficients (italics) will accurately reflect D_{Ra} only if the minerals in our separates are zero-age.

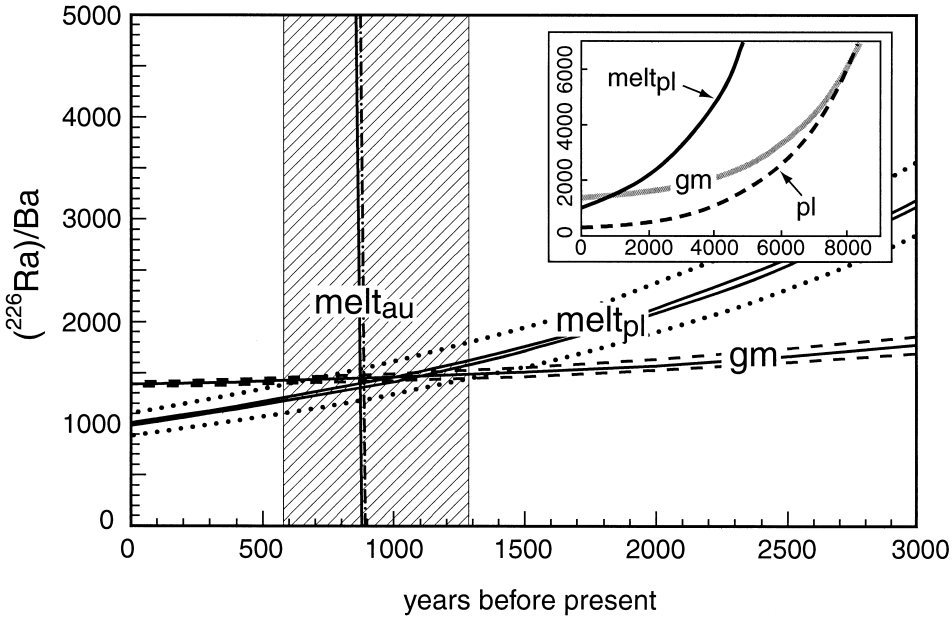

Fig. 5. Diagram showing the variation through time in (^{226}Ra)/Ba of melts in equilibrium with the plagioclase and augite crystals relative to that of the groundmass. Ra is normalized to Ba rather than Th because the ratio D_{Ra}/D_{Ba} is better constrained than D_{Ra}/D_{Th} (because of the charge difference) or than either of the individual partition coefficients (see Appendix B). Solid curves for melt in equilibrium with plagioclase correspond to An_{70} at 1160°C (upper curve) and An_{60} at 1100°C (lower curve); the dotted curves allow for 10% uncertainty in calculated D_{Ra}/D_{Ba} for plagioclase. Dashed lines for groundmass evolution through time indicate propagation of measurement uncertainties. Box with diagonal ruling represents age range of intersection of curves for groundmass and melt in equilibrium with plagioclase. Curves for melt in equilibrium with augite ($melt_{au}$) are also shown, calculated using the Th/Ba ratio measured by ion microprobe and the best-fit (^{226}Ra)/Ba obtained by mass balance considerations based on those same data, together with the partition coefficients in Table 3; solid and dot-dash lines delimit range of curves permitted by ±35% uncertainty in partition coefficients and variations due to temperature. Inset illustrates how the evolution of (^{226}Ra)/Ba in the melt in equilibrium with plagioclase ($melt_{pl}$) would compare to that of plagioclase itself (dashed curve, pl) when the initial fractionation of Ra from Ba is taken into account. The intersection of $melt_{pl}$ and gm curves shows the crystallization age of plagioclase. Increasing the magnitude of Ra–Ba fractionation decreases the age inferred for plagioclase crystallization. See text for discussion.

lower in augite than in plagioclase at the time of crystallization and data for the mineral pair would initially define a negative slope on an isochron diagram.

The difference between initial (^{226}Ra)/Ba predicted by partitioning and that measured in the minerals can be explained by aging of the system subsequent to interelement fractionation by crystallization. However, the initial (^{226}Ra)/Ba of the minerals depends on (^{226}Ra)/Ba in the melt at the time of crystallization. In order to quantify the duration of 'crystal residence', the calculated partition coefficients (Table 3) can be used to model the (^{226}Ra)/Ba values of magmas in equilibrium with those of the augite and plagioclase in the past; the results are shown in Fig. 5. To do so accurately, however, the effect of impurities on the (^{226}Ra)/Ba ratios in the mineral separates must be included in this analysis.

For the plagioclase and augite data to be consistent with co-precipitation from a melt represented by the groundmass, all three curves shown in Fig. 5 ($melt_{au}$, $melt_{pl}$, and gm) should intersect at a point which represents the (^{226}Ra)/Ba ratio of the melt in equilibrium with the two phases and which also delimits the model age of the crystals. As shown by the ruled box in Fig. 5, the melt in equilibrium with the plagioclase would have had (^{226}Ra)/Ba ratios like those in the groundmass at 1000^{+300}_{-400} a, given the uncertainty in calculated

partition coefficients. In this case, the effect of a small proportion of glass in the plagioclase separate ($<0.8\%$) propagates into a relatively small uncertainty in the combined (^{226}Ra)/Ba–(^{230}Th)/Ba characteristics of the plagioclase and therefore in its minimum crystallization age: the age of plagioclase assuming that the separate contains up to 0.8% melt inclusions will be up to $\sim$300 yr greater than that assuming no melt inclusions, comparable to the uncertainty in the age due to propagation of uncertainties in partition coefficients. Therefore, for the purpose of delimiting the minimum crystallization age, we assume no melt inclusions in the plagioclase separate.

In order to accurately apply the partition coefficients calculated for augite, we base our model crystallization ages on the Ra concentration in augite calculated from the foregoing mass balance considerations and on the Th and Ba concentrations obtained from the ion microprobe analyses. Because of its strong enrichment in ^{230}Th with respect to ^{226}Ra, (^{226}Ra)/Ba of augite evolves rapidly away from values which could be in equilibrium with the 1955 groundmass or, for that matter, any other Kilauean basalt (cf. [17,18]). The present-day (^{226}Ra)/Ba of the pyroxene requires $\sim$900 yr of radiogenic ingrowth from a ratio that would be in equilibrium with the groundmass, as indicated by the point of intersection between (^{226}Ra)/Ba evolution curves for groundmass and for melt in equilibrium with the augite. It is worth noting that applying the calculated Ra/Ba partition coefficients directly to (^{226}Ra)/Ba measured in the pyroxene separate (and using (^{230}Th)/Ba data for that separate) would lead to an apparent crystallization age of $\sim$3800 a. The calculated D_{Ra}/D_{Ba} in augite is so low that the uncertainty in this ratio has virtually no effect on the apparent crystallization age (Fig. 5). However, the large uncertainty in Ra concentration in augite, derived from uncertainty in the Ra contribution from the very small quantity of impurities in the pyroxene separate, is permissive of crystallization ages ranging from $\sim$90 to $\sim$2700 a. In all likelihood, however, the initial Ra–Ba fractionation in plagioclase and augite was no greater than that predicted by theoretical partitioning, in which case the minimum model age of $\sim$600 a deduced from our plagioclase data is our best estimate of the minimum average crystal residence time.

4.3. Dated crystals: phenocrysts and/or xenocrysts?

Petrographic and BSE evidence presented here and in previous work [13,15] indicates that few of the silicate crystals have features such as resorbed cores or reverse zoning which would suggest magma mixing and/or introduction of xenocrysts into the melt. The range in augite compositions is consistent with progressive crystallization of the early 1955 magma: the more magnesian augites (Fig. 4) could have crystallized from a melt with Mg/Fe similar to whole rock analyses of vent E [13] whereas, with a few exceptions, the less magnesian augites approach compositions in equilibrium with the glass. Accordingly, the minimum model age of $\sim$600 a for crystallization of plagioclase and augite would represent an average age of crystallization weighted by the volume of crystals produced at a given time. The range in augite compositions could alternatively indicate mixing of two differentiated magma batches (e.g., [14]); in this case, the mean crystallization age would represent a minimum residence time for the older of the two batches. If, however, the separates contain a large fraction of xenocrysts that are remnants from crystallization of a previous batch of *evolved* magma, the mean crystallization age would reflect some contribution from these older crystals. U-series disequilibria uniquely constrain this scenario because xenocrysts older than $\sim$8 ka are essentially in ^{226}Ra–^{230}Th radioactive equilibrium and have a (^{226}Ra)/(^{230}Th) value indistinguishable from unity. The effects of such xenocrysts on the mean age of the mineral separates (and thus on the minimum magma residence time) can be assessed by a simple mixing calculation. Assuming, for example, that plagioclase xenocrysts older than $\sim$8 ka are mixed with zero-age plagioclase which have (^{226}Ra)/Ba like that predicted by calculated partition coefficients, $\sim$30% xenocrysts would have to be present in the plagioclase separate for the residence time of the magma to be negligible. If initial Ra–Ba frac-

tionation in zero-age plagioclase were less than predicted by partitioning, or if the xenocrysts were younger than 8 ka, the percentage of xenocrysts required would be even greater. The various lines of evidence cited here and elsewhere [14] are only permissive of a volumetrically minor quantity of xenocrysts in the lava, so that the (^{226}Ra)/Ba ratio in our separates likely is dominated by crystals grown from this batch of magma. For this reason, the remainder of the discussion will focus on the minimum mean crystal age ($\sim$600 yr) as a measure of the magmatic residence time which, for a magma erupted in 1955, implies a minimum residence time of $\sim$550 yr.

4.4. Residence, cooling, and crystal growth in the reservoir

Studies of crystal size distributions in lava lakes and sills suggest that, within a given part of the reservoir system, average crystal growth rates may not vary much with time [25]. Accordingly, the *mean* crystal age of $\sim$550 yr before eruption, coupled with the assumption of constant growth rates, could indicate that the oldest crystals began to form $\geq$1100 yr before eruption. However, in detail, crystal growth rates inferred from crystal size distributions in basaltic dikes and lava lakes appear to be a function of local cooling rates and thus will vary from one part of the reservoir system to another, and likely will vary from interior to exterior even within a given reservoir [26]. Thus, given the likely possibility that thermal conditions of storage and thus local cooling rates changed during the history of the 1955 magma (for example, when moving from the summit reservoir to the rift reservoir), we base the following calculations of cooling rates and magmatic residence times on the conservative minimum age of $\sim$550 yr for initial crystallization of pyroxene and plagioclase.

Although the relatively evolved composition of the early 1955 magma suggests that its overall thermal history may have been unusual with respect to most Kilauean magmas, the rate at which it cooled was likely representative of the reservoir(s) in which it was stored prior to eruption. For Kilauea, the main conduit feeding the shallow reservoir system appears to supply deep levels of the summit reservoir, which then supplies the rift reservoirs (e.g., [6]). Heat loss from a more isolated and tabular rift zone magma body is likely to be more efficient than that from the more equant geometry inferred for the summit reservoir. The maximum average rate of magma cooling for the early 1955 magma is 0.1°C/yr (1×10^{-5}°C/h) during the period of pyroxene+pla-

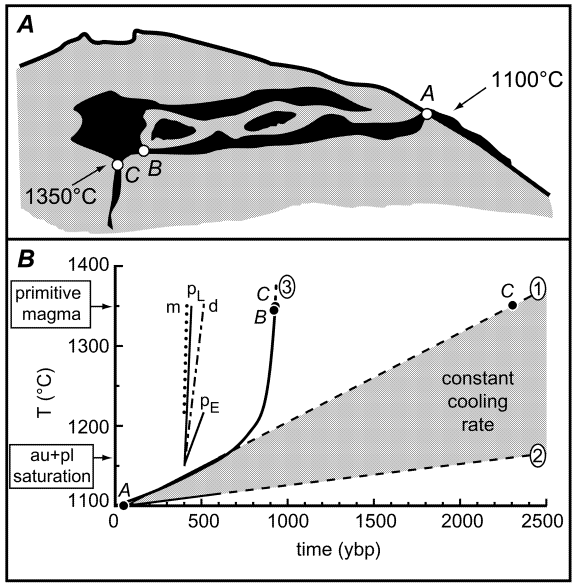

Fig. 6. Thermal history. A: Schematic cross section of the summit and east rift zone of Kilauea, showing magma reservoir system. Letters A–C correspond to magma as it is erupted, magmas moving from the summit reservoir to the rift reservoir, and primitive magma entering the shallow reservoir system, respectively. B: Possible thermal histories for the early 1955 magma, keyed to locations in A. Curves 1 and 2 show linear extrapolations of the maximum and minimum average cooling rates for the early 1955 magma, respectively. Curve 3 is a schematic exponential extrapolation of that cooling rate. Lines labeled with lower-case letters show trends of cooling rates based on residence times of: (m) $\sim$10 yr for the 1959 Kilauea Iki eruption [1]; (d) $\sim$100 yr [3]; and (p_L) 30–40 yr for the late 20th century lavas [2], all shown for cooling from average temperature of primitive magma (1350°C) to representative eruption temperatures. Line p_E uses residence estimate of 90–180 yr for the early 20th century lavas [2] and cooling from 1215°C (corresponding to their minimum estimate of MgO in parental magma) to 1150°C; other combinations of temperature intervals and residence estimates of [2] result in curves with slopes between the two shown. See text for discussion.

gioclase growth, based on the 60°C interval from initial co-precipitation to eruption and the minimum mean age of mineral growth of 550 yr before eruption. This calculation assumes that the minerals analyzed are representative of those which crystallized since the system was initially augite+plagioclase saturated. The bulk composition of the early 1955 lava is, however, much more differentiated than Kilauean glasses in equilibrium with augite+plagioclase at the highest temperature of co-saturation [21]. A reasonable lower limit to the average cooling rate, ~0.05°C/yr, can therefore be obtained by assuming that the average age of 550 yr for crystal growth corresponds to the interval between liquidus (~1125°C; calculated using the whole rock MgO content and the MgO geothermometer of Helz and Thornber [21]) and eruption temperatures for the early 1955 lava (see Fig. 6).

The average temperature of magma entering the crustal reservoir system at Kilauea has been estimated to be ~1350°C [8]. If cooling rates like those we have inferred were constant over the entire thermal interval of magma storage (1350–1100°C), the total storage time of the magma would therefore be greater than 2500 yr (Fig. 6). However, cooling rates are unlikely to be constant over long periods of storage, especially if a magma spends time in both the summit and rift reservoirs. For a magma body isolated throughout most of its cooling history, as might happen in the rift zone, temperature would likely decrease exponentially with time (illustrated schematically in Fig. 6B) as predicted by simple conductive cooling models. If this case applies to the early 1955 magma, the total storage time might be only tens to a few hundreds of years longer than the minimum residence time of the 1955 magma.

Cooling rates that we calculate from the residence estimates obtained in earlier studies of Kilauea [1–3] and the large temperature interval of cooling (from 1350°C to eruption at ~1150°C) are much faster than the average cooling rate calculated for the 1955 magma (Fig. 6B). A striking feature of these cooling rates (e.g., 2–5°C/yr for late 20th century lavas in the 2–3 km^3 summit reservoir [2]) is that they are comparable to or even faster than cooling rates of ~3°C/yr in the small-volume (0.04 km^3) Kilauea Iki lava lake [27]. Even so, the disparity between cooling rates might be reconciled if the earlier estimates are representative in some fashion of the thermal history for magmas beneath the summit area, whereas our cooling rate estimate applies to rift zone storage. However, the implication would be that cooling rates in the summit reservoir are even faster than those in the rift reservoir, the opposite relationship of what would be expected based solely on the inferred shapes and volumes of the two reservoirs.

Uncertainties in the relative cooling rates aside, the fact that our estimate of residence time is longer than most other estimates may still reflect true variations in storage time for different batches of magma (which could be largely averaged out by geochemical and geophysical estimates), and/or may reflect the fact that it is for a relatively differentiated rift zone lava, whereas most other estimates apply to more primitive summit lavas [1–3]. The geochemical estimates [2,5] of magma residence are based on the assumption that temporal fluctuations in geochemistry result from efficient mixing of a chemically distinct primary magma into a reservoir with a different composition. Assuming that this model is correct, residence times of tens of years could be applicable to the most active part of the reservoir system, whereas hundreds of years may be more representative of part of the system peripheral to the main magma conduit. The geophysical estimate of thousands of years [4] could in turn reflect an average of the entire volume of magma within the system. If, on the other hand, we allow for the possibility of inefficient and/or temporally discrete episodes of mixing, the observed chemical and isotopic variations [2] could simply reflect stratification in an ascending magma column and/or tapping and mixing of different volumes of magma within the system, with little to no bearing on residence time. It is notable in this context that, whereas estimates of magma residence in some other basaltic systems (Santorini, Reunion, Mt. Etna, and Iceland) are <100 yr [28–30], recent U-series studies of mafic volcanism at Grande Comore Island [31] and Ardoukoba, Asal rift [32] suggest residence times of the order of 100–650 yr and

870–1880 yr, respectively, which are similar to our results.

In summary, ^{226}Ra–^{230}Th data obtained for plagioclase, pyroxene, and groundmass from the early phase of the 1955 east rift eruption at Kilauea produce a widely scattered array about a ~3 ka apparent isochron if simply plotted on a Ba-normalized ^{226}Ra–^{230}Th isochron diagram. When the disequilibria are considered in light of petrographic observations, in situ trace element measurements, and theoretical partitioning relations, they demonstrate significant fractionation of Ra from Ba during crystallization. Moreover, our data suggest that the effects of this fractionation on the initial isotopic characteristics of minerals can be accounted for by calculations of theoretical partitioning behavior, but age interpretations based on mineral separates must reflect the fact that the separates are not completely pure and therefore that model partition coefficients do not strictly apply to them. When corrections for impurities in the mineral separates are considered, our data are consistent with coprecipitation of plagioclase and clinopyroxene from a melt represented by the groundmass at a mean age of 1000^{+300}_{-400} a, which constrains the minimum residence time to be ~550 yr for all or some of the magma, depending on whether the early 1955 lavas represent an isolated batch of magma or a mixture of differentiated magmas. This estimate is within the range of estimates based on geophysical techniques but is longer than previous estimates of crustal magma residence at Kilauea based on geochemical arguments, which may reflect the fact that the different methods are sampling different parts and/or proportions of the reservoir system. By measuring residence times for specific magmas, and by linking residence times to specific temperature intervals, it should be possible to infer more general thermal characteristics of the magma reservoir system.

Acknowledgements

This work was supported by the Institute of Geophysics and Planetary Physics at Los Alamos National Laboratory (M.T.M. and M.R.R.), and a U.S. Department of Energy, Office of Basic Energy Sciences, Geosciences Research Program grant to M.T.M. D.A.C. thanks the David and Lucile Packard Foundation for their generous support. Sample collection was supported by a Geological Society of America Research grant to K.M.C., and K.M.C. also thanks D. Swanson and J. Kauahikaua for help during field work, R. Roback for help with Ra chemistry, and C. Coath and K. McKeegan for help with the ion microprobe analyses. The manuscript benefited from constructive comments and suggestions by T. Wright, R. Helz. and K. Cashman, by reviewers A. Pietruszka, T. Elliott, and by an anonymous reviewer.*[FA]*

Appendix A. Analytical methods

A.1. Sample collection and preparation

The lava sample used in this study was collected just south of Highway 132, between vents E and J (nomenclature of Macdonald and Eaton [11]). Because the two vents are close together were simultaneously active, it is likely that the same magma erupted from both vents and therefore analyses of vent E material are representative of our sample. Separates of plagioclase and pyroxene (4–6 g) were prepared from the 250–600 μm size fractions using standard magnetic and density methods followed by hand-picking. In order to further purify the plagioclase separate, it was crushed to ~60–100 μm and magnetically separated from glass. The pyroxene separate was treated with a cold, dilute (1–2%) HF solution for 2–4 h in an ultrasonic bath to remove glass adhering to the outside of grains, and additional hand-picking was performed to remove grains which still had visible glass. All samples were cleaned ultrasonically in successive baths of acetone, distilled water, 0.1 M oxalic acid+2% H_2O_2, 0.1 M HCl+2% H_2O_2, Teflon-distilled water, and distilled acetone, then air-dried under clean-lab conditions at LANL. Samples were digested in a concentrated HCl/HF mixture, evaporated and redissolved in 3 M HCl, centrifuged, and repeat-

edly treated with perchloric and nitric acids until no visible residue remained after centrifuging.

A.2. TIMS measurements

All chemical separations and TIMS analyses were performed under clean-lab conditions at LANL. Solutions were split into three aliquots for isotopic analysis, which were spiked with ^{134}Ba, with ^{229}Th and ^{233}U–^{236}U, and with ^{228}Ra, respectively. Ba in the first aliquot was purified using cation exchange resin, loaded onto a single outgassed Re filament with silica gel, and analyzed dynamically on a single ion-counting detector. Ba concentrations were obtained from measured ^{134}Ba/^{138}Ba ratios corrected for Ba blanks (total-process blanks were <12 ng Ba, $<2\%$ of the smallest sample analyzed), and instrumental fractionation relative to natural ^{135}Ba/^{138}Ba = 0.09194 using ^{135}Ba/^{138}Ba ratios measured during the run.

Aliquot containing Th and U spikes was purified using anion exchange resin with nitric acid. After purification, Th and U were loaded together on single Re filaments between layers of graphite. Corrections were made for blanks (Th blanks <0.5 ng Th, U blanks 10–60 pg U for these measurements and for Th and U isotopic measurements described below); neglecting this correction changes the Th concentrations by $\sim 1\%$ for whole rock and groundmass and $\sim 10\%$ for minerals and results in $<1\%$ change in calculated U concentrations for all samples.

Th and U isotopic measurements were performed on the Ra-spiked solution. Th and U were pre-concentrated using anion exchange resin with nitric acid and were separated from each other using anion exchange resin and hydrochloric and sulfuric acids. Th and U fractions were each purified further with a final nitric acid anion column and were run in triple-filament assemblies with Re center filaments and Re (Th) or Ta (U) side filaments.

Washes from the first anion column in the Th/U isotopic procedure were collected, and Ra was purified using cation exchange resin (NH_4^+ form) with 0.01 M EDTA as the eluant, using procedures modified from [39]. Sample sizes were ~ 150 fg ^{226}Ra for whole rock and groundmass samples, and 5–10 fg ^{226}Ra for mineral separates. Backgrounds at masses 228 and 226 were less than 1 cps (generally <0.5 cps) for pyroxene and plagioclase analyses and 1–2 cps for whole rock and groundmass analyses. Blanks for Ra were lower than the detection limit (~ 0.1 fg) and thus represent $<1\%$ of the plagioclase and whole rock/groundmass samples, and $<2\%$ of the pyroxene sample. Measured ^{226}Ra/^{228}Ra ratios were corrected for ^{226}Ra in the spike and for ^{228}Ra in equilibrium with ^{232}Th in the sample.

A.3. Ion microprobe analyses of Th and Ba concentration in pyroxene

A polished, Au-coated grain mount was prepared from a split of the same pyroxene separate used for TIMS work. Ba and Th were analyzed using a CAMECA ims 1270 high resolution ion microprobe at UCLA. Samples were run with 23 nA primary beam current ($^{16}O^-$ beam) and a -30 V offset during Ba analysis to minimize molecular interferences, at a mass resolving power of ~ 4000. Spot size was ~ 40 μm in diameter (cf. Fig. 3). ^{138}Ba and ^{232}Th^{16}O counts were normalized to ^{28}Si. Count rates were 0.4–0.7 and 0.5–10 cps for ThO and ^{138}Ba, respectively, in augite unknowns. Th and Ba concentrations in unknowns were calculated by calibrating with respect to the weighted mean of ^{138}Ba/^{28}Si and ^{232}Th^{16}O/^{28}Si ratios in three ion microprobe analyses of Washington University glass standard WU-A using the concentrations of Th (0.0529 ± 0.0012 ppm) and Ba (1884.5 ± 2.3 ppm) measured in WU-A by INAA (R. Korotev, personal communication; 1σ errors). ^{30}Si/^{28}Si values were also monitored during analysis, and the measured ratio was always within 2% of the natural ratio. ^{137}Ba/^{138}Ba values measured in glass standards and in augite grains during the same analysis session as the unknowns were within analytical error (2σ) of the natural ratio. Accuracy of Th measurements was assessed by analyzing NBS SRM 614 (0.748 ppm) and SRM 616 (0.0252 ppm) as unknowns and these gave values within 15% and

within measurement error (2σ) of the standard value, respectively.

Appendix B. Calculation of partition coefficients and estimated uncertainties

We calculated partition coefficients for Ra and Ba in plagioclase using equation 3 of Blundy and Wood [22], which calculates the partition coefficient for an element of interest (D_i) relative to an element with a known partition coefficient D_a, based on the variables E (Young's modulus of the crystal site of substitution) and r_0 (ideal site radius). Partition coefficients in this model are sensitive primarily to temperature and crystal composition (which affect E and r_0); we used a range of plagioclase compositions from An_{60}–An_{70}, based on the composition of the majority of plagioclase analyses for the early 1955 lavas reported in [40], and temperatures ranging from initial saturation of augite+plagioclase at 1160 ± 10°C to eruption at 1100 ± 10°C, calculated using the MgO geothermometer of [21] and the glass compositions measured by [15].

Because E, r_0, and D_a are functions of the composition of the crystal and of temperature (and to a lesser extent, of pressure), they will be constant for any cation of a given charge substituting into a given crystal. Therefore, uncertainties in the *ratio* of partition coefficients for two isovalent cations will be independent of D_a and will depend only on the uncertainties in E and r_0. We used values calculated assuming that E and r_0 vary linearly between end-member plagioclase compositions, after Blundy and Wood [22], with uncertainties based on the standard deviations of experimental measurements for their regression. Allowing E and r_0 to vary by two standard deviations and propagating these variations through equation 3 results in a change of less than 10% (relative) in the ratio D_{Ra}/D_{Ba}.

We calculated partition coefficients for augite using equation 10 in Wood and Blundy [24] (corresponding to equation 3 in [22]). We used their equation 14 to calculate E (corrected for 2+ ions as described in [24]) with the same range in temperatures discussed above and pressure of 0.1 GPa, consistent with a magma chamber depth of ~2–4 km; the calculation is relatively insensitive to direct effects of pressure. We calculated r_0 using their equation 15 with the average of our electron microprobe measurements of augite composition (SiO_2, 51.56; MgO, 16.30; Na_2O, 0.24; Al_2O_3, 2.63; FeO, 8.75; MnO, 0.22; Cr_2O_3, 0.17; CaO, 18.79; TiO_2, 1.10; in wt%). Wood and Blundy found that >92% of the D values for clinopyroxene calculated using their model fell within 0.73 and 1.36 times the experimentally determined partition coefficients. Moreover, because the experimental measurements of concentrations generally had relative errors of 20–50% (1σ) themselves, this spread may be due as much to uncertainties in the experimental measurements as to uncertainties in the model calculations [24]. As with plagioclase, the uncertainty in the ratio of two partition coefficients will be less than the uncertainty in each absolute value; therefore, 35% is a generous estimate of the relative 2σ uncertainty in our calculation of D_{Ra}/D_{Ba} for augite. Thus, the uncertainty in the ratio of two partition coefficients will be less than 10% for plagioclase and less than 35% for augite, as long as there are no major influences on partitioning behavior that are not accounted for in the model.

References

[1] M.T. Mangan, Crystal size distribution systematics and the determination of magma storage times: The 1959 eruption of Kilauea volcano, Hawaii, J. Volcanol. Geotherm. Res. 44 (1990) 295–302.
[2] A.J. Pietruszka, M.O. Garcia, The size and shape of Kilauea Volcano's summit magma storage reservoir: a geochemical probe, Earth Planet. Sci. Lett. 167 (1999) 311–320.
[3] R.W. Decker, Dynamics of Hawaiian volcanoes: an overview, in: R.W. Decker, T.L. Wright, P.H. Stauffer (Eds.), Volcanism in Hawaii, U.S. Geological Survey Professional Paper 1350 2, 1987, pp. 997–1018.
[4] R.P. Denlinger, A dynamic balance between magma supply and eruption rate at Kilauea volcano, Hawaii, J. Geophys. Res. 102 (1997) 18091–18100.
[5] M.O. Garcia, J.M. Rhodes, F.A. Trusdell, A.J. Pietruszka, Petrology of lavas from the Puu Oo eruption of Kilauea Volcano: III. The Kupianaha episode (1986–1992), Bull. Volcanol. 58 (1996) 359–379.
[6] M.P. Ryan, The mechanics and three-dimensional internal

structure of active magmatic systems: Kilauea Volcano, Hawaii, J. Geophys. Res. 93 (1988) 4213–4248.
[7] T.L. Wright, R.S. Fiske, Origin of the differentiated and hybrid lavas of Kilauea Volcano, Hawaii, J. Petrol. 12 (1971) 1–65.
[8] D.A. Clague, J.G. Moore, J.E. Dixon, W.B. Friesen, Petrology of submarine lavas from Kilauea's Puna Ridge, Hawaii, J. Petrol. 36 (1995) 299–349.
[9] P.T. Delaney, R.S. Fiske, A. Miklius, A.T. Okamura, M.K. Sato, Deep magma body beneath the summit and rift zones of Kilauea Volcano, Hawaii, Science 247 (1990) 1311–1316.
[10] R.S. Fiske, W.T. Kinoshita, Inflation of Kilauea Volcano prior to its 1967–1968 eruption, Science 165 (1969) 341–349.
[11] G.A. Macdonald, J.P. Eaton, Hawaiian volcanoes during 1955, U.S. Geol. Surv. Bull. 1171 (1964) 1–170.
[12] T.L. Wright, Chemistry of Kilauea and Mauna Loa Lava in Space and Time, U.S. Geological Survey Professional Paper, 1971, 40 pp.
[13] R. Ho, M.O. Garcia, Origin of differentiated lavas at Kilauea Volcano, Hawaii: Implications from the 1955 eruption, Bull. Volcanol. 50 (1988) 35–46.
[14] R.T. Helz, T.L. Wright, Differentiation and magma mixing on Kilauea's east rift zone: a further look at the eruptions of 1955 and 1960. Part I. The late 1955 lavas, Bull. Volcanol. 54 (1992) 361–384.
[15] A.T. Anderson, T.L. Wright, Phenocrysts and glass inclusions and their bearing on oxidation and mixing of basaltic magmas, Kilauea Volcano, Hawaii, Am. Mineral. 57 (1972) 188–216.
[16] A.M. Volpe, P.E. Hammond, ^{238}U–^{230}Th-^{226}Ra disequilibria in young Mount St. Helens rocks: time constraint for magma formation and crystallization, Earth Planet. Sci. Lett. 107 (1991) 475–486.
[17] A.J. Pietruszka, K.H. Rubin, M.O. Garcia, ^{226}Ra–^{230}Th-^{238}U disequilibria of historical Kilauea lavas (1790–1982) and the dynamics of mantle melting within the Hawaiian plume, Earth Planet. Sci. Lett. (in press).
[18] K.W.W. Sims, D.J. DePaolo, M.T. Murrell, W.S. Baldridge, S. Goldstein, D. Clague, M. Jull, Porosity of the melting zone and variations in solid mantle upwelling rate beneath Hawaii: Inferences from ^{238}U–^{230}Th–^{226}Ra and ^{235}U–^{231}Pa disequilibria, Geochim. Cosmochim. Acta 63 (1999) 4119–4138.
[19] M.K. Reagan, A.M. Volpe, K.V. Cashman, ^{238}U- and ^{232}Th-series chronology of phonolite fractionation at Mount Erebus, Antarctica, Geochim. Cosmochim. Acta 56 (1992) 1401–1407.
[20] S.J. Schaefer, N.C. Sturchio, M.T. Murrell, S.N. Williams, Internal ^{238}U-series systematics of pumice from the November 13, 1985, eruption of Nevado del Ruiz, Colombia, Geochim. Cosmochim. Acta 577 (1993) 1215–1219.
[21] R.T. Helz, C.R. Thornber, Geothermometry of Kilauea Iki lava lake, Hawaii, Bull. Volcanol. 49 (1987) 651–668.
[22] J. Blundy, B. Wood, Prediction of crystal-melt partition coefficients from elastic moduli, Nature 372 (1994) 452–454.
[23] P. Beattie, Systematics and energetics of trace-element partitioning between olivine and silicate melts Implications for the nature of mineral/melt partitioning, Chem. Geol. 117 (1994) 57–71.
[24] B.J. Wood, J.D. Blundy, A predictive model for rare earth element partitioning between clinopyroxene and anhydrous silicate melt, Contrib. Mineral. Petrol. 129 (1997) 166–181.
[25] B.D. Marsh, On the interpretation of crystal size distributions in magmatic systems, J. Petrol. 39 (1998) 553–599.
[26] K.V. Cashman, Relationship between plagioclase crystallization and cooling rate in basaltic melts, Contrib. Mineral. Petrol. 113 (1993) 126–142.
[27] R.T. Helz, Kilauea Iki: a model magma chamber (abstract), Eos Trans. Am. Geophys. Union 72 (Suppl.) (1991) 315.
[28] F. Albarede, Residence time analysis of geochemical fluctuations in volcanic series, Geochim. Cosmochim. Acta 57 (1993) 615–621.
[29] O. Sigmarsson, Short magma chamber residence time at an Icelandic volcano inferred from U-series disequilibria, Nature 382 (1996) 440–442.
[30] G. Zellmer, S. Turner, C. Hawkesworth, Timescales of destructive plate margin magmatism: new insights from Santorini, Aegean volcanic arc, Earth Planet. Sci. Lett. 174 (2000) 265–281.
[31] C. Claude-Ivanaj, B. Bourdon, C. Allegre, Ra–Th–Sr isotope systematics in Grande Comore Island: a case study of plume–lithosphere interaction, Earth Planet. Sci. Lett. 1998 (1998) 99–117.
[32] N. Vigier, B. Bourdon, J.L. Joron, C.J. Allegre, U-decay series and trace element systematics in the 1978 eruption of Ardoukoba, Asal rift: timescale of magma crystallization, Earth Planet. Sci. Lett. 174 (1999) 81–97.
[33] V.A.M. Langenheim,D.A. Clague, The Hawaiian-Emperor volcanic chain, Part II: Stratigraphic framework of volcanic rocks of the Hawaiian Islands, in: R.W. Decker, T.L. Wright, P.H. Stauffer (Eds.), Volcanism in Hawaii, U.S. Geological Survey Professional Paper 1350 1, 1987, pp. 55–84.
[34] T.L. Grove, M.B. Baker, Phase equilibrium controls on the tholeiitic versus calc-alkaline differentiation trends, J. Geophys. Res. 89 (1984) 3253–3274.
[35] C.C. Lundstrom, H.F. Shaw, F.J. Ryerson, D.L. Phinney, J.B. Gill, Q. Williams, Compositional controls on the partitioning of U, Th, Ba, Pb, Sr, and Zr between clinopyroxene and haplobasaltic melts: implications for uranium series disequilibria in basalts, Earth Planet. Sci. Lett. 128 (1994) 407–423.
[36] P. Beattie, The generation of uranium series disequilibria by partial melting of spinel peridotite: constraints from partitioning studies, Earth Planet. Sci. Lett. 117 (1993) 379–391.
[37] T.Z. LaTourrette, D.S. Burnett, Experimental determination of U and Th partitioning between clinopyroxene and

natural and synthetic basaltic liquid, Earth Planet. Sci. Lett. 110 (1992) 227–244.
[38] T. Dunn, C. Sen, Mineral/matrix partition coefficients for orthopyroxene, plagioclase, and olivine in basaltic to andesitic systems: A combined analytical and experimental study, Geochim. Cosmochim. Acta 58 (1994) 717–733.
[39] A.M. Volpe, M.T. Murrell, Determination of radium isotope ratios and abundances in geologic samples by thermal ionization mass spectrometry, Anal. Chem. 63 (1991) 913–916.
[40] T.L. Wright, R.T. Helz, Differentiation and magma mixing on Kilauea's east rift zone: a further look at the eruptions of 1955 and 1960, Part II, The 1960 lavas, Bull. Volcanol. 57 (1996) 602–630.